8 Biological Science

8-1 X-ray Crystallography of Kinesin Motors

Molecular motors are enzymes that convert energy liberated by chemical reactions into mechanical works. Kinesin superfamily proteins are a family of molecular motors most of which transport several organelles along their cellular track microtubules by using the energy of ATP hydrolysis [1]. Recently, some kinesins are shown to destabilize the microtubule from its both ends for reorganizing their cellular track, or for mitosis [2]. To elucidate the molecular mechanism of the translational movement along microtubules and the microtubule destabilization, we have solved crystal structures of these two types of kinesins: KIF1A [3] as a transporter and KIF2C [4] as a microtubule destabilizer using PF BL-6A and AR-NW12 beamlines.

Crystal structures of the transporter KIF1A were solved in ATP state (with ATP analog, AMPPNP) and in two ADP-phosphate states (transition state of ATP hydrolysis; with two classical ADP-phosphate analogs, ADP-AlFx and ADP-vanadate), and were compared with the known structure in ADP state [5] (Fig. 1). These structures computationally docked with microtubules showed that KIF1A uses two microtubule-binding loops, L11 and L12, in an alternating manner during ATP hydrolysis. In the ATP state, KIF1A extends the loop L11 and is strongly bound to the microtubule. During ATP hydrolysis (ADP-phosphate states), KIF1A transiently raises both microtubule-binding loops (L11 and L12), thus actively detaching itself from the microtubules. After hydrolysis (ADP state), KIF1A extends another loop L12 to the microtubules. Since this L12 interacts with the flexible C-terminal region named E-hook of microtubule, this flexible binding allows diffusive movement of KIF1A along microtubules. These structural results are very consistent with the KIF1A movement directly visualized by the single molecule analysis [6, 7].

The overall architecture of the microtubule destabilizer KIF2C was very similar to the transporter KIF1A (Fig. 2a). However, large structural differences were found in the following three class specific regions: the class-specific N-terminal neck, the loop L2, and the loop L8. Since all these regions directly face to the microtubule, the microtubule-interface of KIF2C is very different from that of KIF1A; KIF1A fits very well with the straight protofilament of microtubule, whereas KIF2C fits with the curved protofilament of microtubule (Fig. 2b, c). Microtubule protofilament naturally takes straight conformation in its side wall and curved conformation at its both ends. Thus, when KIF2C reaches to the end of microtubule, KIF2C makes full contact with curved protofilament of microtubule. Then, N-terminal neck region, inserting deeply into the interprotofilament groove, destabilizes the lateral interaction of the protofilament. Also, the loops L2 (KVD finger) and L8 cooperatively stabilize the curved protofilament at the both ends of the microtubule. These effects are enough to shift the microtubule dynamics to depolymerization without further active processes.

Finally, we note that KIF2C as well as KIF1A use the energy of ATP hydrolysis for the detachment from the microtubule, which enables KIF2C continuously destabilizing the microtubule. This design principle of the active detachment from its effecter molecule is similar to that of G-proteins, protein kinases, and other nucleotidases. In other words, the energy of hydrolysis is used for their active detachment which is necessary to cycle the reaction such as the signal transduction, the movement along the microtubule, or the microtubule destabilization. This conserved strategy might reflect the evolutionary pathway of these classes of proteins.

R. Nitta[1], T. Ogawa[1], M. Kikkawa[1,2], Y. Okada[1] and N. Hirokawa[1] ([1]Univ. of Tokyo, [2]Univ. of Texas)

References

[1] N. Hirokawa, *Science,* **279** (1998) 519.
[2] N. Homma, Y. Takei, Y. Tanaka, T. Nakata, S. Terada, M. Kikkawa, Y. Noda and N. Hirokawa, *Cell,* **114** (2003) 229.
[3] R. Nitta, M. Kikkawa, Y. Okada and N. Hirokawa, *Science,* **305** (2004) 678.
[4] T. Ogawa, R. Nitta, Y. Okada and N. Hirokawa, *Cell,* **116** (2004) 591.
[5] M. Kikkawa, E.P. Sablin, Y. Okada, H. Yajima, R.J. Fletterick and N. Hirokawa, *Nature,* **411** (2001) 439.
[6] Y. Okada and N. Hirokawa, *Science,* **283** (1999) 1152.
[7] Y. Okada, H. Higuchi and N. Hirokawa, *Nature,* **424** (2003) 574.

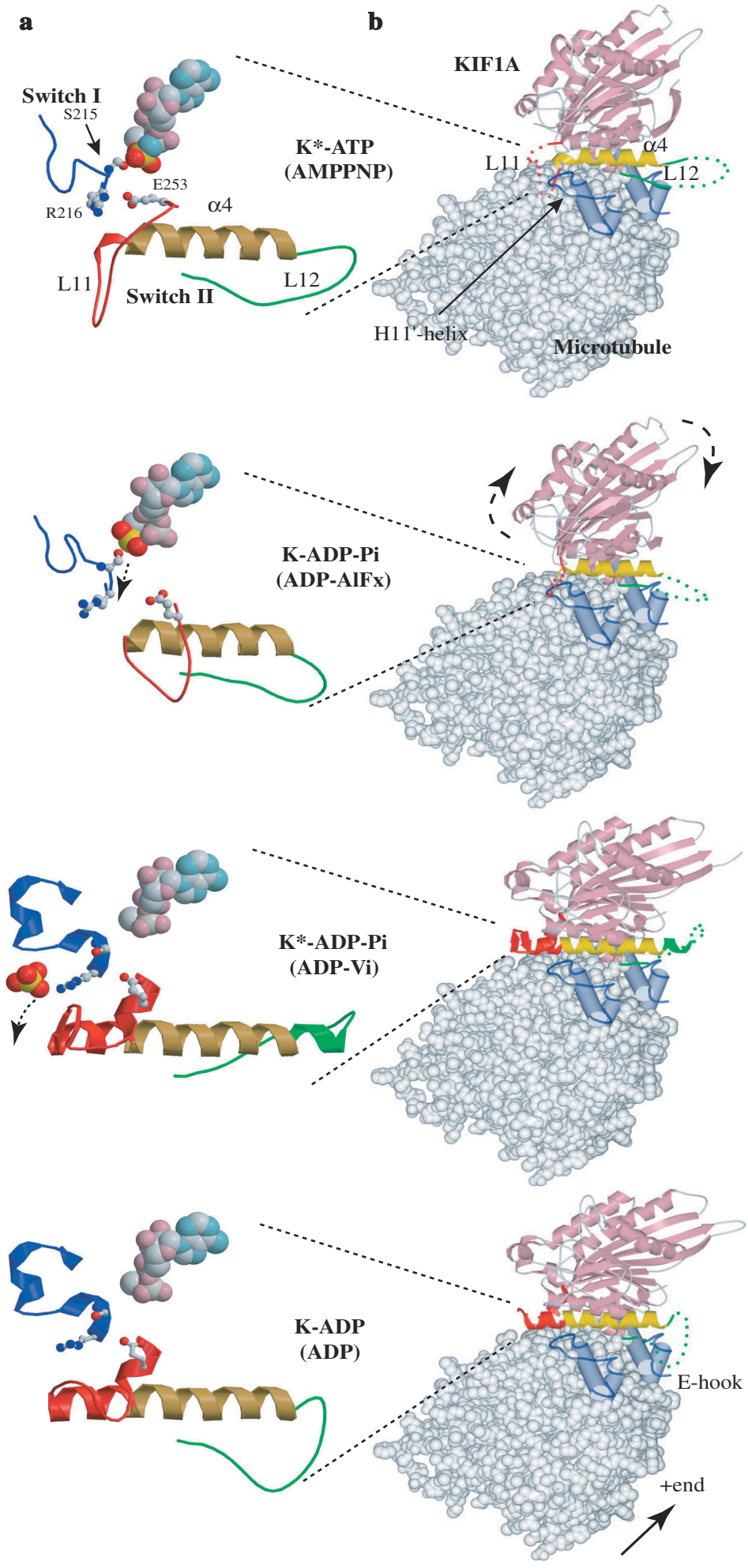

Figure 1
Hydrolysis-induced conformational changes of KIF1A. Panel (a) schematically illustrates the conformational changes of KIF1A. The switch I region (blue) and the switch II cluster (L11 in red, α4 in yellow, and L12 in green) are shown as ribbon models. Nucleotides are shown as space-filling models. The residues important for γ-phosphate release (S215, R216 and E253) are shown as ball-and-stick models. (b) KIF1A-microtubule complex seen from the minus end of the microtubule. The microtubules (gray) are shown as space-filling models except for the helices H11, H12 and the E-hook (blue).

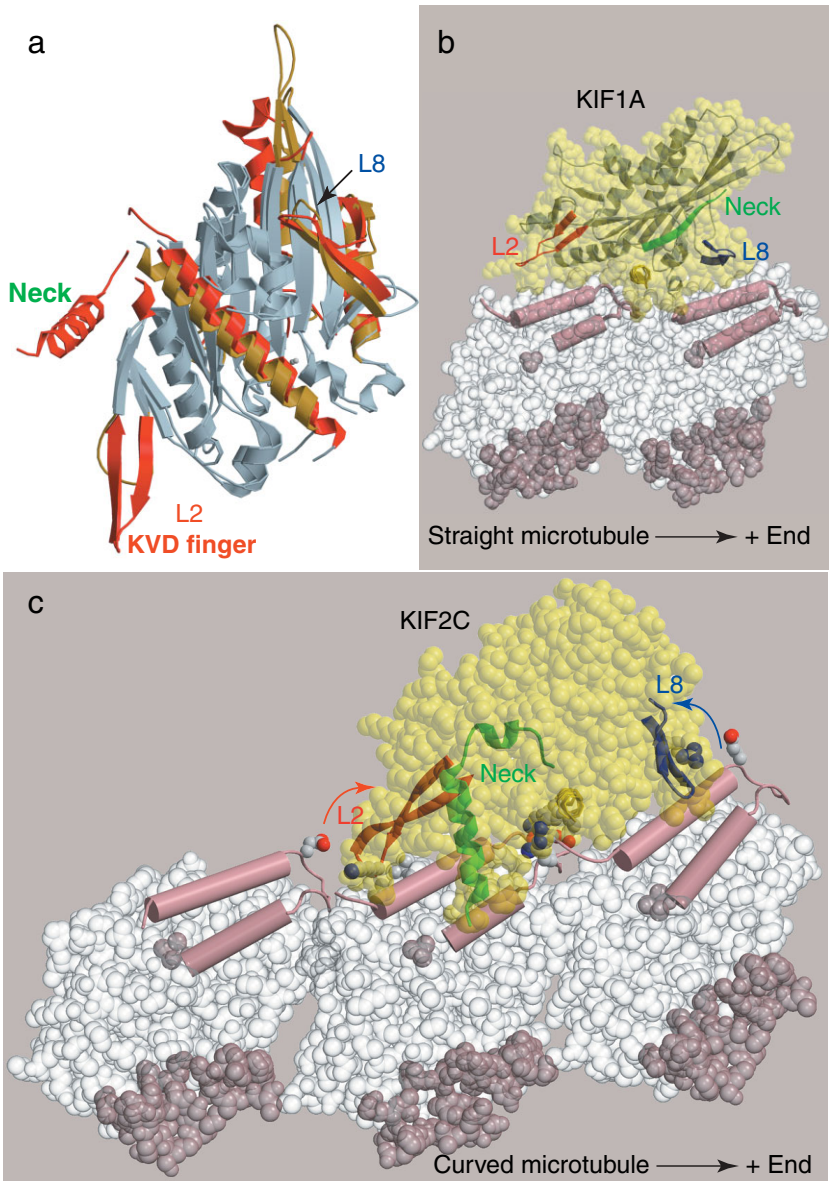

Figure 2
In silico modeling to dock the atomic models of KIF1A and KIF2C to that of the microtubule protofilament. (a) Comparison of the structure of KIF2C with that of KIF1A seen from the microtubule binding side. The overlapping structures are colored with gray. The highly divergent structural elements of KIF2C and KIF1A are colored with red and yellow, respectively. (b) Docking of KIF1A (yellow) to the straight microtubule protofilament (white). H11 and H12 of tubulin are shown as brown cylinders, and the M-loop is shown in dark-brown. (c) Docking of KIF2C (yellow) to the curved protofilament. The interface of KIF2C fits very well with curved protofilament and the loops L2 and L8 cooperatively stabilize the curved protofilament (red and blue allows).

8-2 Three-dimensional Structure of Spinach Major Light-harvesting Complex

The major light-harvesting complex of photosystem II (LHC-II) functions as principal solar energy collector in photosynthesis of green plants and may also have a role in photoprotection under high-light conditions. The electron crystallographic model of pea LHC-II at 3.4 Å resolution, reported in 1994, revealed some basic structural features of LHC-II [1]. In the past ten years, researchers has been eagerly awaiting for the structure of LHC-II at higher resolution, so that the processes of light harvesting and energy transfer in plant photosynthesis as well as the mechanism of photoprotection can be understood at complete atomic details.

We have determined the structure of LHC-II at 2.72 Å resolution by X-ray crystallography [2]. The diffraction data were collected at beamlines BL-6B of PF and 3W1A of BSRF (Beijing, China). One asymmetric unit of a huge *R*32 unit cell ($a = b = 261.8$ Å, $c = 660.5$ Å) contains ten LHC-II monomers. Every twenty LHC-II trimers in complex with lipids and detergents are assembled into a unique icosahedral proteoliposome (Fig. 3a). The icosahedral vesicle, with an outer diameter of about 261 Å and an inner diameter of about 160 Å, serves as basic structural element of the crystal unit cell (Fig. 3b). This is a novel way of membrane protein crystallization, named 'Type III'.

The basic structural and functional unit of LHC-II is the trimer (Fig. 4). Hydrophobic interactions dominate the associations between adjacent monomers within a trimer. Fourteen chlorophyll (Chl) molecules have been determined within a monomer. For the first time, they were unambiguously distinguished as eight Chl*a* and six Chl*b*. The transition dipole moment of each chlorophyll has been accurately assigned.

Several interesting chlorophyll arrangement characteristics of LHC-II have been unraveled (Fig. 4). Firstly, all chlorophylls are vertically distributed into two layers within the membrane (Fig. 4b). Within a

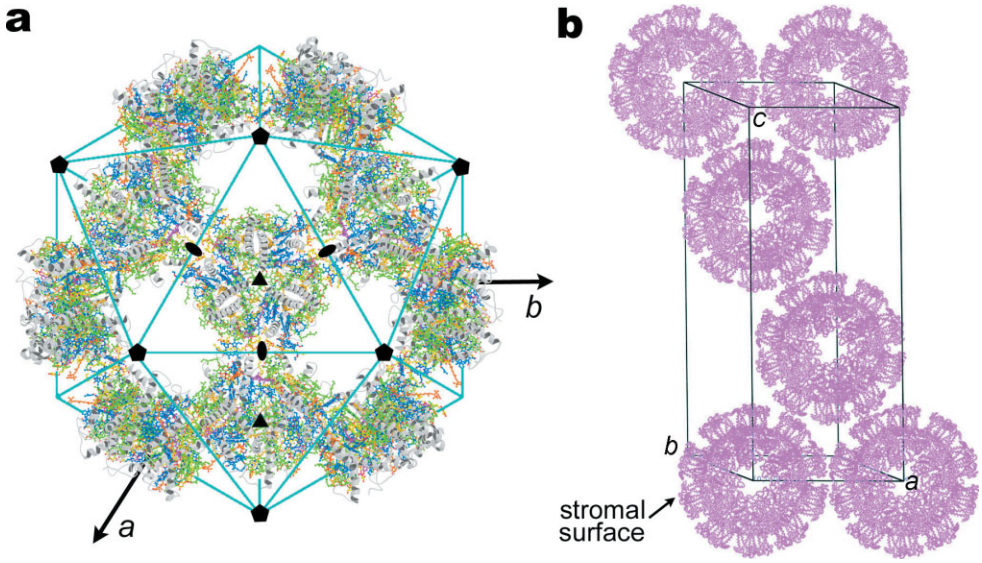

Figure 3
An icosahedral vesicle and the crystal packing. (a), One-half of the vesicle viewed along the c-axis of the hexagonal cell. (b), Packing diagram of 'Type III' membrane-protein crystal.

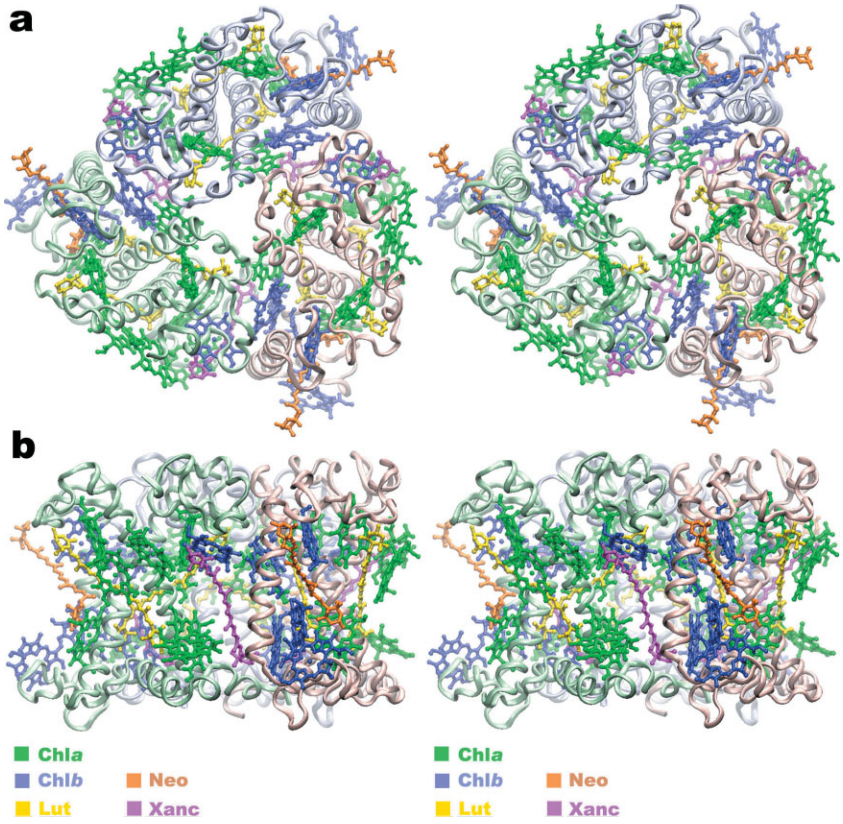

Figure 4
Stereo view of a LHC-II trimer. Ribbons, polypeptides; ball-and-stick models, prosthetic groups. The chlorophyll phytyl chains and lipids are omitted for clarity. Abbreviations: Chla, chlorophyll a; Chlb, chlorophyll b; Lut, lutein; Neo, neoxanthin; Xanc, xanthophyll-cycle carotenoid. (a), Top view along the membrane normal from the stromal side. (b), Side view in parallel with the membrane plane.

monomeric LHC-II, the eight chlorophylls at the stromal side form an elliptical ring, whereas the remaining six chorophylls at the lumenal side aggregate into two separate clusters. Secondly, all Chl*b* are located around the interface between adjacent monomers (Fig. 4a), which might be of critical importance in energy equilibrating inside a functional trimer. Thirdly, 24 chlorophylls from the stromal layer of the trimeric LHC-II are organized into two irregular circular rings. The inner ring composed of six Chl*a* molecules are proposed to have an important role in inter-monomeric energry transfer. The novel mosaic arrangement pattern of the pigment in outer ring would not only favor the efficient absorption of incident light energy from all directions in a broad spectral region, but also facilitate the transfer of the excitation energy to the nearest exit. The chlorophyll clusters at lumenal side, separated by larger distances, might serve as upstream energy collectors.

Four carotenoid binding sites per monomeric LHC-II were observed (Fig. 4). The xanthophyll-cycle carotenoid

at the monomer-monomer interface may be involved in the non-radiative dissipation of excessive energy, one of the photoprotective strategies evolved in plants. Finally, we proposed a structure-based non-photochemical quenching model by combining the structural evidences with the results of functional research [2].

Z.F. Liu, H.C. Yan, K.B. Wang, T.Y. Kuang, J.P. Zhang, L.L. Gui, X.M. An and W.R. Chang (Chinese Academy of Sciences)

References

[1] W. Kühlbrandt, D.N. Wang, and Y. Fujiyoshi, *Nature,* **367** (1994) 614.
[2] Z.F. Liu, H.C. Yan, K.B. Wang, T.Y. Kuang, J.P. Zhang, L.L. Gui, X.M. An and W.R. Chang, *Nature,* **428** (2004) 287.

8-3 Crystal Structure and Molecular Mechanism of Transcription Factor DksA

Stringent control, which is a complex of regulatory events in bacterial cell starved for amino acids, is triggered by the elevated concentrations of guanosine-tetraphosphate (ppGpp, known also as ”magic spot”). Complexed with RNA polymerase (RNAP), this nucleotide selectively regulates transcription of genes involved in amino acid metabolism. On one hand, ppGpp inhibits transcription of rRNA and tRNA genes, on the other, it stimulates expression of proteins required for amino acid biosynthesis and transport. The overall effect of ppGpp action is thus to increase amino acid pools in the cell.

An intriguing and unresolved discrepancy exists between small albeit reproducible ppGpp effects in highly purified *in vitro* systems and the dramatic range of regulation observed *in vivo*. This apparent discrepancy could be due to a requirement for cellular factor(s) that modulate ppGpp activity *in vivo* – in fact, the existence of such an auxiliary factor was proposed nearly 30 years ago. Recently, the DksA protein was shown to greatly amplify inhibition of rRNA transcription by ppGpp *in vitro,* and thus DksA may play a role of a missing *in vivo* modulator of the ppGpp activities.

Recently, we solved the 2.0 Å resolution X-ray structure of bacterial (*Escherichia coli*) DksA protein using PF-AR NW12 beamline [1]. We show a surprising result that DksA protein, lacking any sequence similarity, closely resembles in structure another well known transcription factor GreA. Both contain a long α-helical coiled-coil domain with invariant acidic residues at the tip. It was proposed recently that upon binding to RNAP, GreA protrudes deeply its coiled-coil domain into the substrate entry (secondary) channel towards the RNAP active site, where its invariant acidic residues coordinate catalytic Mg^{2+} ion.

We have already determined the RNAP/ppGpp complex structure [2], which revealed that ppGpp binds in the RNAP secondary channel in a close vicinity to the RNAP active site. The structure also identified two Mg^{2+} ions bound to each di-phosphates of ppGpp. Whereas one of the ppGpp-bound Mg^{2+} ions is buried within the protein and is well fixed by the protein residues, the second Mg^{2+} ion is accessible from the outside through the RNAP

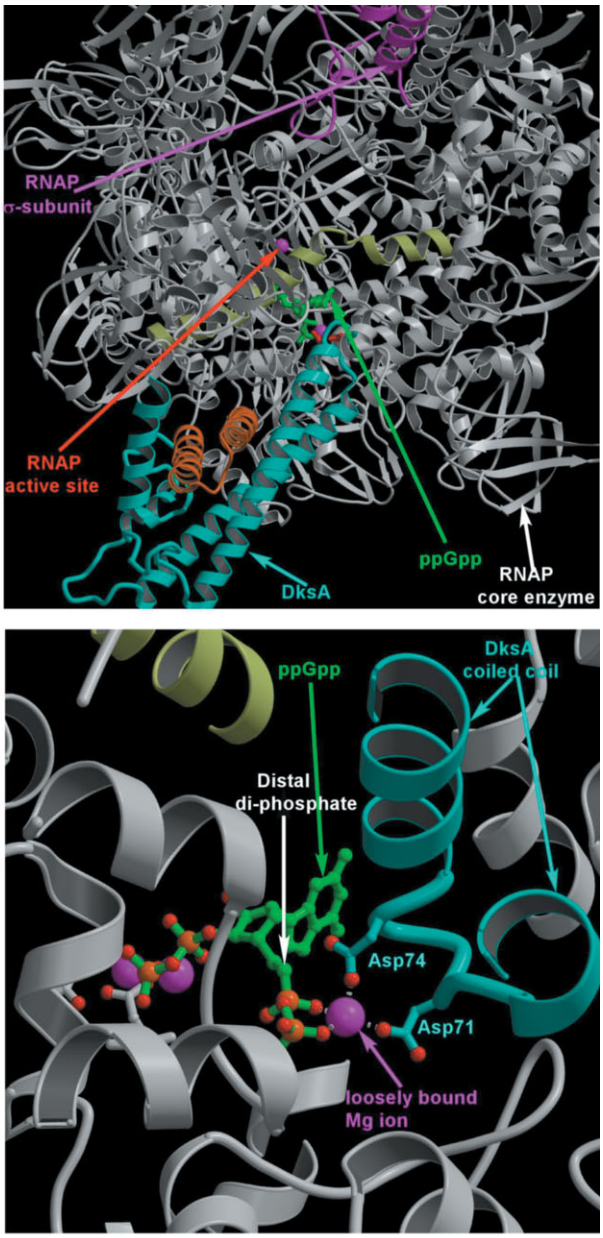

Figure 5
Upper panel. Model of the RNAP/DksA/ppGpp complex (overview)
Lower panel. Close up view of the ppGpp binding site of the RNAP/DksA/ppGpp complex.

secondary channel and is loosely bound by only ppGpp phosphates.

Given the previously demonstrated modulation of ppGpp activity by DksA and structural similarity with GreA, the DksA structure implies the molecular mechanism, in which DksA, like GreA, binds to RNAP, protrudes its coiled-coil domain through the secondary channel towards ppGpp biding site, and stabilizes RNAP/ppGpp complex through coordination of the loosely ppGpp-bound Mg^{2+} by the invariant acidic residues (Fig. 5). To

verify the proposed mechanism we have carried out a limited set of the focused biochemical experiments that showed that DksA indeed directly binds to RNAP positioning the tip of its coiled-coil domain near the RNAP active site, and that invariant acidic residues are crucial to the DksA function - mutations of these residues resulted in loss of the DksA effect on the ppGpp activity. Thus the secondary channel emerges as a common regulatory entrance for transcription factors.

A. Perederina[1], V. Svetlov[2], M.N. Vassylyeva[1,3], T.H. Tahirov[1], S. Yokoyama[1,3,4], I. Artsimovitch[2] and D.G. Vassylyev[1] ([1]RIKEN Harima Inst., [2]Ohio State Univ., [3]RIKEN GSC, [4]Univ. of Tokyo)

References

[1] A. Perederina, V. Svetlov, M.N. Vassylyeva, T.H. Tahirov, S. Yokoyama, I. Artsimovitch and D.G. Vassylyev, *Cell*, **118** (2004) 297.

[2] I. Artsimovitch, V. Patlan, S. Sekine, M.N. Vassylyeva, T. Hosaka, K. Ochi, S. Yokoyama and D.G. Vassylyev, *Cell*, **117** (2004) 299

8-4 The Atomic Structure of *Rice Dwarf* Virus

Rice dwarf virus (RDV), a causal agent of rice dwarf disease, is a member of the genus *Phytoreovirus* in the family *Reoviridae*. It is transmitted to rice, wheat, barley, and other gramineae plants by insect vectors, with the main vectors being leafhoppers (*Nephotettix* species), after multiplication of the virus in the insect. Infection by RDV results in chlorotic specks on leaves and stunting of plant growth. RDV is prevalent and it is one of the viruses that cause the most economic damage in China, Japan and other Asian countries. Each viral particle is an icosahedral shape of approximately 700 Å in diameter [1], consisting of two concentric layers of proteins that encapsidate a genome of 12 discrete double-stranded (ds)RNAs (Fig. 6). The core particle is composed of P1, a putative RNA polymerase; P5, a putative guanylyltransferase; and P7, a non-specific nucleic acid-binding protein. The core is encapsidated with a thin layer of P3 core capsid proteins. The outer layer of the virus is composed of mainly P8 proteins, with a small number of P2 proteins, which are required for vector transmission. Particles with only P8 in their outer layer can infect to insect vectors via needle injection, while core particles with P2 and P8 proteins can infect insect vectors by needle infection and by membrane feeding. The total molecular mass of a particle is about 70 million Dalton (Fig. 6).

We have solved the atomic structure of RDV, determined at 3.5 Å resolution by X-ray crystallography using PF BL-6A, 6B and 18B [2]. The model consists of P3 inner capsid proteins (Fig. 7a), P8 outer capsid proteins (Fig. 7b), and fragments of P7, the nucleic acid binding protein. The atomic structure suggests a self-assembly mechanism for both homologous (P3-P3 and P8-P8) and heterologous (P3-P8) capsid proteins. A hierarchy of structural organization of this double-shelled virus is proposed on the basis of inter-subunit inter-atomic distances and the electrostatic surface potentials of the various subunits. Insertion of the amino-terminal arm of one P3 protein (P3B) into another P3 protein (P3A) was found to be essential for the dimeric association of this core capsid protein (Fig. 8a). The interaction between two P3 proteins alters the conformation of the amino-terminal region of one of the P3 proteins. Ten residues in the amino-terminal region block the extension of the amino-terminal loop of the other protein (Fig. 8a). This interaction triggers an overall structural change in the latter P3 protein to form

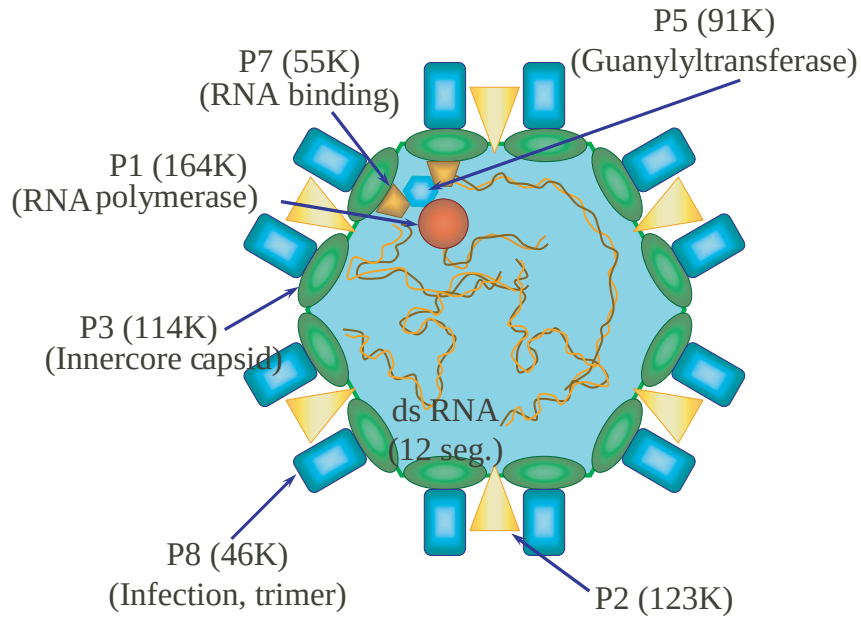

Figure 6
Components of RDV particle. Numbers in parenthesis are molecular weights of the proteins.

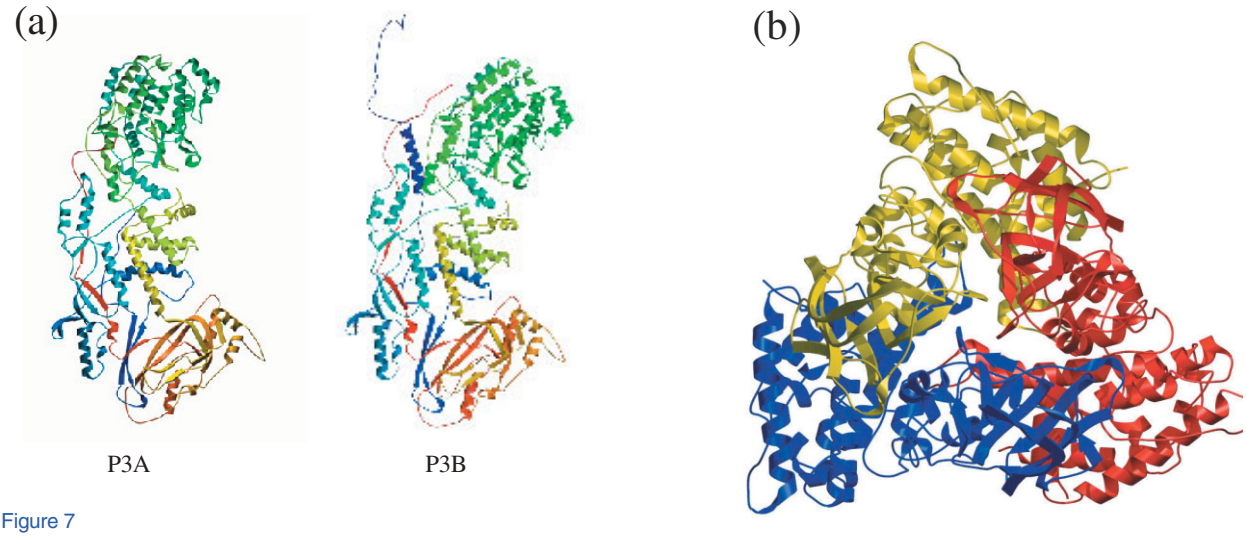

Figure 7
Ribbon drawing of the component proteins. (a) Core capsid protein, P3. Two icosahedrally independent P3 proteins P3A (Left) and P3B (Right), have similar but significantly different overall shapes. (b) Trimer structure of outer capsid protein, P8. Although 13 icosahedrally different subunit structures were found in the outer shell, all structures were basically the same (r.m.s. deviations between each subunits were less than 1 Å).

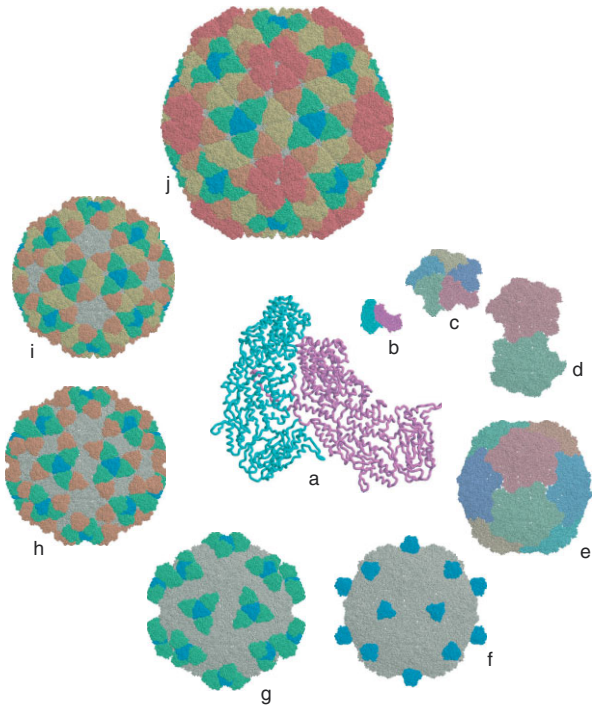

Figure 8
Proposed hierarchy for the assembly of RDV particle. On the basis of the apparent interactions between the various proteins, we propose the following sequence of events. (a) Insertion of the amino-terminal arm of P3B (pink) into P3A (light blue) initiates the assembly of a P3 dimer. (b) This P3A-P3B dimer acts as a unit piece in the jigsaw puzzle. (c) A pentameric structure of dimers of P3 protein forms around an icosahedral 5-fold axis, and then (d) this pentameric structure assembles (e) to form the core structure of an RDV particle. The trimeric structure of P8 proteins acts as a unit of the outer capsid. The outer capsid consists of five kinds of P8 trimers (T, S, R, Q and P) which are icosahedrally independent. (f) The T-trimer (blue) attach to the icosahedral three-fold axis first. Orientation of the T-trimer on the surface of the core is defined by electrostatic complementarities. (g) R-trimers (green) then attach via interactions with the inner shell and with the T-trimers. (h) Q-trimers (orange) and (i) S-trimers (yellow) attach to the core surface and at the final stage of viral assembly, (j) P-trimers (red) attach at the icosahedral 5-fold axes to form the complete virus particle.

tight coupling of the two P3 molecules. This dimeric structure initiates the assembly of the inner core of the virus (Fig. 8b-e). The interactions between the P3 core capsid protein and the P8 outer capsid protein involve predominantly hydrogen bonds and electrostatic interactions, with surface-charge complementarity. The interactions among P8 trimers involve side-by-side contacts among trimers. The surface of P8 trimers has clear positively and negatively charged patches, which exhibit complementarity in terms of electrostatic charges with adjacent P8 trimers, which can, thus, associate to form the outer capsid layer of the virus (Fig. 8f-j). The proposed model for the hierarchy of structural assembly is shown schematically in Fig. 8.

A. Nakagawa[1], N. Miyazaki[1], J. Taka[1], H. Naitow[1], A. Ogawa[1], Z. Fujimoto[2], H. Mizuno[2], T. Higashi[3], Y. Watanabe[3], T. Omura[3], R.H. Cheng[4] and T. Tsukihara[1]
([1]Osaka Univ., [2]Nat. Inst. Agr. Sci., [3]Nat. Agr. Res. Cen., [4]Karolinska Inst.)

References

[1] H. Mizuno, H. Kano, T. Omura, M. Koizumi, M. Kondoh and T. Tsukihara, *J. Mol. Biol.,* **219** (1991) 665.
[2] A. Nakagawa, N. Miyazaki, J. Taka, H. Naitow, A. Ogawa, Z. Fujimoto, H. Mizuno, T. Higashi, Y. Watanabe, T. Omura, R. H. Cheng and T. Tsukihara, *Structure,* **11** (2003) 1227.

8-5 The Substrate Recognition Mechanism of a Glucuronyltransferase, GlcAT-P, Required for HNK-1 Carbohydrate Biosynthesis

Carbohydrate molecules on cell surfaces modulate a variety of cellular functions, including cell-to-cell interactions [1,2]. The HNK-1 carbohydrate epitope, which is recognized by HNK-1 monoclonal antibodies, is found on many neural cell adhesion molecules and is thought to be required for the development of brain and nerve systems.

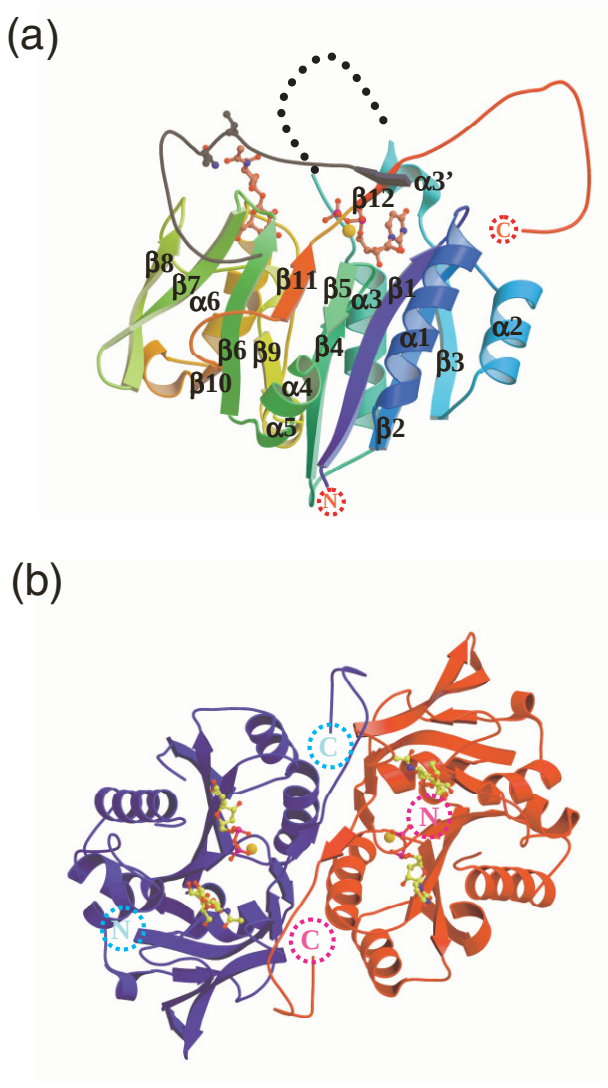

Figure 9
The structure of GlcAT-P in complex with Mn^{2+}, UDP and *N*-acetyllactosamine. (a) Monomer structure of the GlcAT-P quaternary complex. The secondary structures are labeled. UDP, Mn^{2+} and *N*-acetyllactosamine molecules are shown as ball-and-stick models colored according to atom types (nitrogen, blue; carbon, black; oxygen, red; phosphorous, purple; manganese, orange). The C-terminal region of the neighbor molecule is shown in gray. (b) Dimer structure of the GlcAT-P quaternary complex. Molecule A is shown in blue and molecule B is shown in red. UDP, Mn^{2+} and *N*-acetyllactosamine molecules are shown as ball-and-stick models.

It has been reported that there are two mammalian glucuronyltransferases, GlcAT-P and GlcAT-S, which are associated with the biosynthesis of the HNK-1 carbohydrate epitope [3]. Another glucuronyltransferase, GlcAT-I, whose acceptor substrate is proteoglycan has also been characterized [4]. These enzymes catalyze the transfer of glucuronic acid (GlcA) from a donor substrate, uridine diphosphoglucuronic acid (UDP-GlcA), to a reducing terminal residue of oligosaccharide chain in the presence of manganese. There are many differences in substrate specificity of acceptor sugars among them. To elucidate the acceptor substrate specificity of GlcAT-P, we have solved the crystal structures of GlcAT-P with and without substrates using the PF-AR NW12 beamline [5].

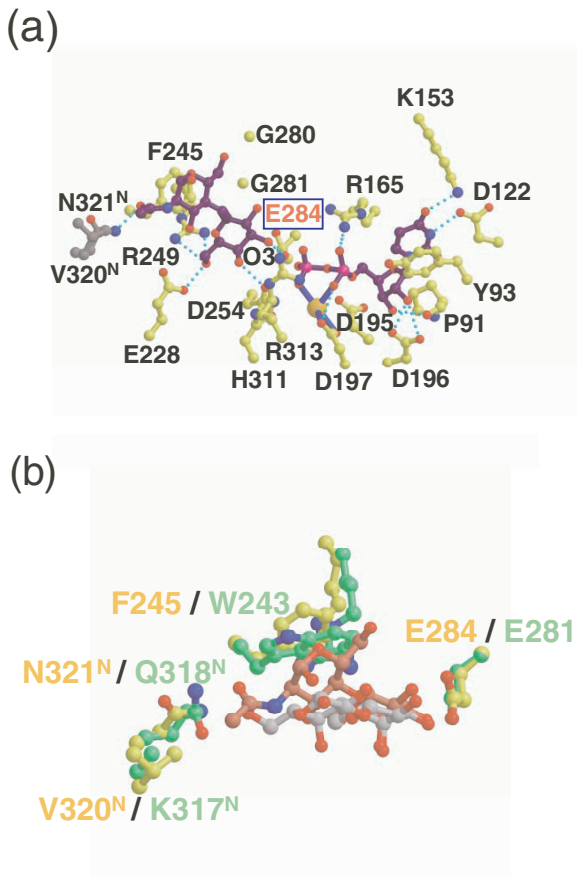

Figure 10
Substrate recognition of GlcAT-P. (a) The three dimensional structure around the active site of GlcAT-P is shown. The amino acid residues of GlcAT-P which interact with substrates and Mn^{2+} are shown in yellow. The superscript "N" denotes residues of the neighboring molecule B (shown in dark gray). UDP and *N*-acetyllactosamine molecules are shown as purple ball-and-stick models colored according to atom types (nitrogen, blue; carbon, black; oxygen, red; phosphorous, purple) and Mn^{2+} ion is colored orange. Hydrogen bonds and metal interactions are represented as dashed and solid light-blue lines, respectively. (b) Comparison of the GlcAT-P quaternary complex (UDP, Mn^{2+} and *N*-acetyllactosamine) with the GlcAT-I quaternary complex (UDP, Mn^{2+} and Galβ1-3Gal) around the acceptor substrate binding site. Residues of GlcAT-P, which are involved in the interaction with the substrates or Mn^{2+}, are shown in yellow. The corresponding residues of GlcAT-I are shown in green. *N*-acetyllactosamine (substrate for GlcAT-P) and Galβ1-3Gal (substrate for GlcAT-I) are shown in orange-red and light gray, respectively. The GlcAT-P and GlcAT-I residues are labeled in yellow and green, respectively.

The overall structure of GlcAT-P consists of twelve β-strands and seven α-helices (Fig. 9a). The N-terminal region (β1-α1-β2-α2-β3-α3'-α3-β4), referred to as a UDP-GlcA binding region, contains an α/β Rossmann-like fold. The C-terminal region (β5-α4-β6-β7-β8-β9-α5-α6-β10-β11-β12), referred to as an acceptor substrate binding region, contains two β-sheets. The C-terminal long loop, which extends to another molecule, is related by the non-crystallographic two-fold axis (Fig. 9b). A UDP moiety of UDP-GlcA which is a donor substrate is recognized with tyrosine (Y93), arginine (R165), aspartic acid (D197), histidine (H311) and arginine (R313) (Fig. 10a, right half region). All these residues are conserved among GlcAT-P, GlcAT-S and GlcAT-I not only on their primary sequences but also on their stereochemical dispositions.

Many amino acid residues (especially the acidic residues; glutamic acid (E228), aspartic acid (D254) and glutamic acid (E284) in GlcAT-P) interact with the acceptor sugar substrate analogue, N-acetyllactosamine (Galβ1-4GlcNAc), in GlcAT-P (Fig. 10a, left half region). These residues are conserved in GlcAT-P, GlcAT-S and GlcAT-I. However, there are some differences among these enzymes. First, the crystal structure of the GlcAT-P complex shows that the C-terminal long loop from the neighbor molecule serves as the key in the recognition of N-acetyllactosamine. Two amino acid residues, valine (V320) and asparagine (N321) of the C-terminal long loop from the neighboring molecule, interact with the GlcNAc residue through a hydrophobic interaction (valine) and a hydrogen bond (asparagine), respectively. V320 is found only in GlcAT-P, not in GlcAT-S nor GlcAT-I. N321 is conserved in GlcAT-P and GlcAT-S, not in GlcAT-I. We propose that this C-terminal long loop is critical for the acceptor specificity. Second, phenylalanine (F245) is important for the interaction with the acceptor substrate, N-acetyllactosamine. GlcAT-S and GlcAT-I have tryptophan at the position corresponding to F245 of GlcAT-P. Although a similar aromatic interaction was found between tryptophan (W243) of GlcAT-I and the galactose ring of the acceptor substrate, both the aromatic ring of W243 and the galactose ring are tilted by 30 degrees keeping their parallelism as compared to those in GlcAT-P (Fig. 10b). These differences in the C-terminal residues of the neighboring molecule, stacking between an aromatic residue and galactose ring account for the differences in the specificity of the substrate acceptor recognition.

T. Shiba[1], S. Kakuda[2], S. Oka[2], T. Kawasaki[2], S. Wakatsuki[1] and R. Kato[1] ([1] KEK-PF, [2] Kyoto Univ.)

References

[1] U. Rutishauser, A. Acheson, A.K. Hall, D.M. Mann and J. Sunshine, *Science,* **240** (1988) 53.
[2] T. M. Jessell, M.A. Hynes and J. Dodd, *Annu. Rev. Neurosci.*, **13** (1990) 227.
[3] S. Oka, K. Terayama, C. Kawashima and T. Kawasaki, *J. Biol. Chem.*, **267** (1992) 22711.
[4] L.C. Pedersen, T.A. Darden and M. Negishi, *J. Biol. Chem.*, **277** (2002) 21869.
[5] S. Kakuda, T. Shiba, M. Ishiguro, H. Tagawa, S. Oka, Y. Kajiwara, T. Kawasaki, S. Wakatsuki and R. Kato, *J. Biol. Chem.*, **279** (2004) 22693.

8-6 Molecular Mechanism of the Glucose Sensor, Human Glucokinase

Glucokinase (hexokinase IV or D) is a cytoplasmic enzyme that phosphorylates glucose and triggers glucose utilization and metabolism. Glucokinase expressed in liver and pancreas is thought to be the glucose sensor controlling plasma glucose levels [1]. The role of glucokinase as a glucose sensor is due to its allosteric properties. The activity of glucokinase exhibits a sigmoidal glucose dependency of which the inflexion point is comparable to plasma glucose levels of normal subjects (Fig. 11). The rapidly increased activity above the normal glucose level ultimately stimulates insulin secretion in pancreatic β-cells and enhances hepatic glucose-uptake and glycogen synthesis. Both of these effects in turn reduce plasma glucose levels. Then, these effects are rapidly disappeared while the plasma glucose level is maintained in the normal range.

Although the allosteric property of glucokinase is critical in glucose homeostasis, the molecular mechanism of this glucose sensor has yet to be elucidated. Structural analyses of oligomeric allosteric proteins, such as hemoglobin, have been extensively studied and clearly showed that the concerted model (MWC model) well explained the positive cooperativity of oligomeric allosteric proteins. But such a mechanism does not appear to be employed by glucokinase because glucokinase is monomeric enzyme with a single active site.

In order to elucidate the molecular mechanism, we analyzed the crystal structures of human glucokinase in both its active and inactive forms [2]. Data collection

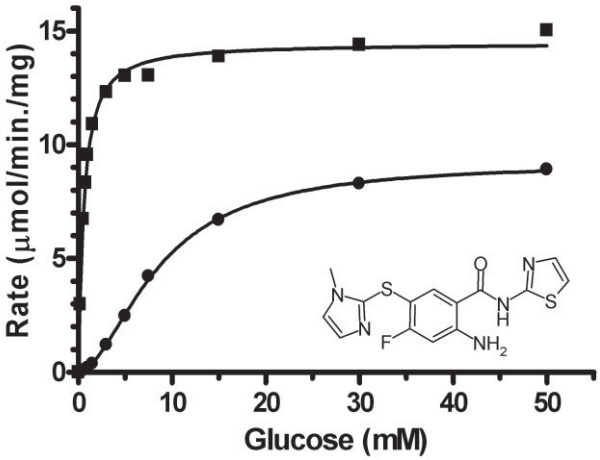

Figure 11
Saturation curve for glucose in the absence (solid circle) and presence of compound A (solid square, 30 μM). Chemical formula of compound A (inset).

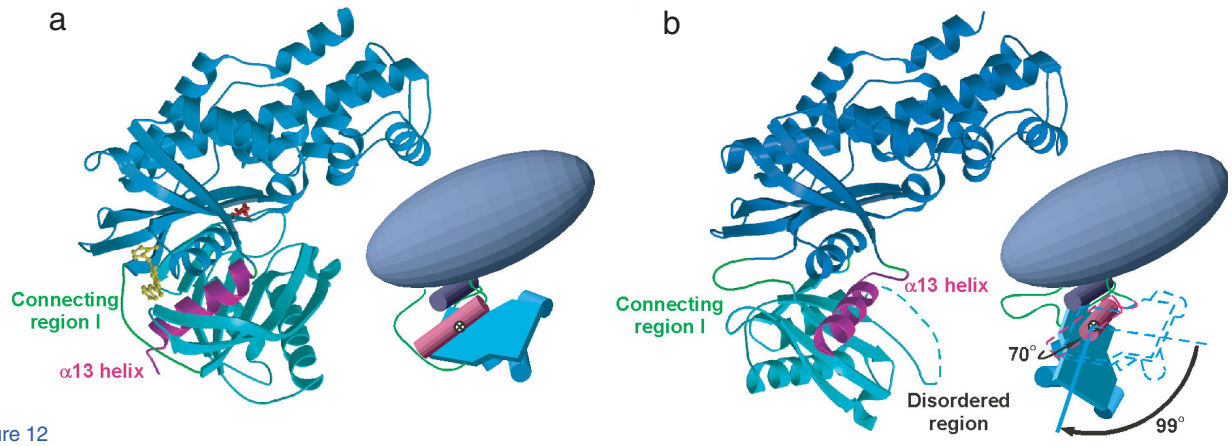

Figure 12
Overall structures of glucokinase. (a) Ribbon drawing (left) and schematic representation (right) of the active form of glucokinase complexed with glucose (red, ball and stick model) and compound A (yellow, ball and stick model). The spatial relationship of the large domain (blue) and the small domain (cyan) exhibited a closed form. The two domains are connected by connecting regions I ~ III (green). The α13-helix (magenta) is included in the small domain of the closed form. (b) The inactive form of glucokinase shown as the same style as (a). The spatial relationship of two domains was designated as the super-open form. The α13-helix is released from the small domain in the super-open form.

was performed at BL-6B and other synchrotron radiation facility. The active conformation of glucokinase was determined in complex with glucose and a synthetic activator, compound A. Compound A is an allosteric activator and changes the shape of the glucose saturation curve from sigmoidal to a hyperbolic curve (Fig. 11). The active structure of glucokinase is almost identical to the closed form of other hexokinases except for the compound A binding site. Hexokinases are isozymes of glucokinase but do not show the positive cooperativity for glucose binding. In the case of hexokinases, the spatial relationship between a large domain and a small domain is changed from an open form to a closed form by the binding of glucose. Although the active form of glucokinase is almost identical to the closed form of hexokinase, inactive form of glucokinase showed a very different overall conformation from the open form of hexokinase. The main part of the small domain was rotated about 99 degrees when compared to the active form. (Fig. 12) This is much larger than 12 degrees rotation observed in closed – open conformational change of hexokinase. Surprisingly, the organization of the small domain was also different in the inactive form. As shown in Fig. 12, the α13 helix, which is the C-terminal region of glucokinase, is part of the small domain in the active form, but it was released from the small domain and lies between the two domains in the inactive form. These results strongly suggest that the positive cooperativity of monomeric glucokinase obeys the "mnemonical mechanism" [3].

Recently, strong allosteric activators such as compound A have been identified by several groups [4,5]. Crystal structures clearly showed that the activation mechanism of compound A is due to the inhibition of the conformational change to the inactive form by the binding to the allosteric site.

K. Kamata, M. Mitsuya, T. Nishimura, J. Eiki and Y. Nagata (Banyu Pharmaceutical Co.,Ltd.)

References

[1] F.M. Matschinsky, B. Glaser, and M.A. Magnuson, *Diabetes,* **47** (1998) 307.
[2] K. Kamata, M. Mitsuya, T. Nishimura, J. Eiki and Y. Nagata, *Structure,* **12** (2004) 429.
[3] M.A. Moukil and E. Van Schaftingen, *J. Biol. Chem.,* **276** (2001) 3872.
[4] J. Grimsby, R. Sarabu, W.L. Corbett, N.E. Haynes, F.T. Bizzarro, J.W. Coffey, K.R. Guertin, D.W. Hilliard, R.F. Kester, P.E. Mahaney, L. Marcus, L. Qi, C.L. Spence, J. Tengi, M.A. Magnuson, C.A. Chu, M.T. Dvorozniak, F.M. Matschinsky, and J.F. Grippo, *Science,* **301** (2003) 370.
[5] K.J. Brocklehurst, V.A. Payne, R.A. Davies, D. Carroll, H.L. Vertigan, H.J. Wightman, S. Aiston, I.D. Waddell, B. Leighton, M.P. Coghlan and L. Agius, *Diabetes,* **53** (2004) 535.

8-7 Crystal Structures of ADP-dependent Glucokinases in Novel Glycolytic Pathway of Hyperthermophilic Archaea

ATP plays universal roles in the transfer and storage of free energy in biological systems as the most common phosphoryl donor for kinases. All known ATP-dependent hexokinases from a wide range of organisms, such as human isozymes I-IV (isozyme IV is also called glucokinase) and yeast isozymes A/B are highly related. However, certain hyperthermophilic archaea, such as *Thermococcus litoralis* and *Pyrococcus furiosus*, utilize unusual ADP-dependent glucokinases (ADPGKs), phosphofructokinases (ADPPFKs), and cupin-type phosphoglucose isomerases (PGIs) in their glycolytic pathways [1]. ADPGKs and ADPPFKs exhibit significant similarity, and form a novel ADP-dependent kinase family. Because no other kinases that use ADP are known to date, this novel kinase group is a very rare example that can shed light on the evolutionary origin of kinases.

We have already solved the first crystal structure of ADPGK from *T. litoralis* (tlGK) complexed with ADP at 2.3 Å resolution (Fig. 13a) [2], using BL-6A, BL-6B, and BL-18B at KEK-PF. The overall structure can be divided into

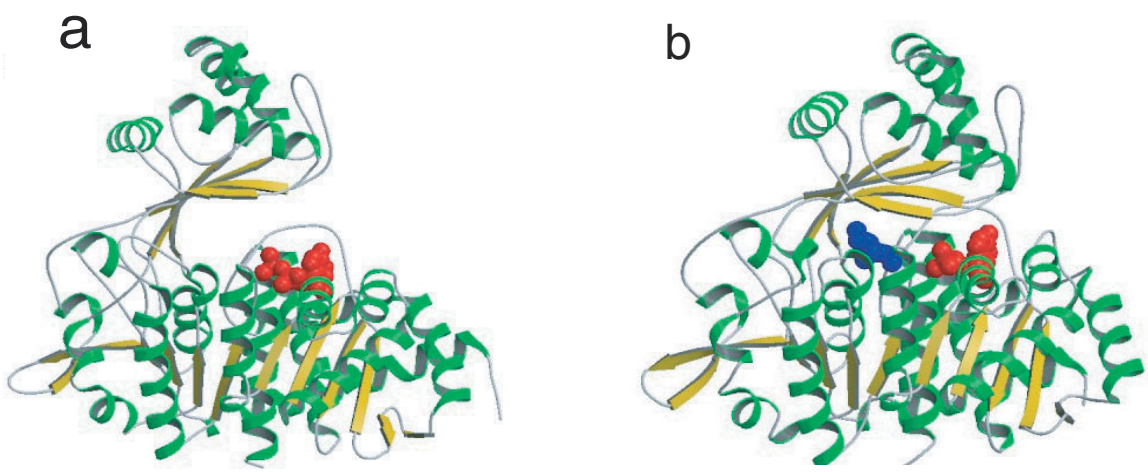

Figure 13
Overall structures of (a) tlGK complexed with ADP (red) in a semi-open form, and (b) pfGK complexed with AMP (red) and glucose (blue) in a closed form. Binding of glucose induces domain closing of ADP-dependent kinase, and then the small domain covers the active center from the solvent.

large and small domains, and the ADP molecule is bound to the large domain. Overall shape of the molecule is similar to conventional ATP-dependent hexokinases, but its fold is completely different. Instead, ADPGK exhibits significant structural similarity with a certain ATP-dependent ribokinase family. Structural comparison between these ADP- and ATP-dependent kinases revealed that the recognition of the α and β-phosphate of ADP in tlGK was almost identical with that of the β and γ-phosphate of ATP in ATP-dependent kinases. In other words, its rare nucleotide specificity is caused by a shift in the nucleotide binding position by one phosphate unit.

Recently, we solved the crystal structure of another ADPGK, the one from *P. furiosus* (pfGK), in a closed conformation complexed with AMP and glucose at 1.9 Å resolution (Fig. 13b) [3], using BL-6A at KEK-PF. In comparison with the tlGK structure, pfGK shows significant conformational changes in the small domain and a region around the hinge. Therefore, three conformations of ADPGKs have been revealed in total (open form, ADPGK from *P. horikoshii* with no ligands [4]; semi-open form, tlGK with ADP; closed form, pfGK with AMP and glucose), suggesting domain closing induced by ADP and glucose. Preliminary crystal structure of ADPPFK from *T. litoralis* was also solved by the MIR method [5]. The overall structure resembles those of ADPGKs, and seems to have an open conformation. In conclusion, although ADP-dependent kinases and conventional ATP-dependent hexokinases comprise of completely different fold, they share similar induced-fit mechanism with domain closing on substrate binding, in order to mask the active center form the solvent.

Archaeal cupin-type PGIs are distantly related to PGIs in general organisms, but rather homologous to the cupin superfamily, which is a group of functionally diverse proteins. The cupin domain consists of a β-structure with six strands, and conserved three histidine and one glutamine residues act as ligands for binding of an active-site metal ion, such as Fe, Mn, or Zn. We recently revealed that the iron is essential for the catalytic activity of PGI from *T. litoralis* [6]. We also solved its crystal structure complexed with iron and glucose-6-phosphate or fructose-6-phosphate.

S. Ito[1], J.-J. Jeong[2], S. Fushinobu[2] and T. Wakagi[2]
([1]Univ. of Shizuoka, [2]Univ. of Tokyo)

References

[1] C.H. Verhees, S.W.M. Kengen, J.E. Tuininga, G.J. Schut, M.W. W. Adams, W.M. de Vos and J. van der Oost, *Biochem. J.,* **375** (2003) 231.
[2] S. Ito, S. Fushinobu, I. Yoshioka, S. Koga, H. Matsuzawa and T. Wakagi, *Structure,* **9** (2001) 205.
[3] S. Ito, S. Fushinobu, J.-J. Jeong, I. Yoshioka, S. Koga, H. Shoun and T. Wakagi. *J. Mol. Biol.,* **331** (2003) 871.
[4] H. Tsuge, H. Sakuraba, T. Kobe, A. Kujime, N. Katunuma and T. Oshima, *Protein Sci.,* **11** (2002) 2456.
[5] J.-J. Jeong, S. Fushinobu, S. Ito, H. Shoun and T. Wakagi, *Acta Cryst. D,* **59**, (2003) 1327.
[6] J.-J. Jeong, S. Fushinobu, S. Ito, B.-S. Jeon, H. Shoun and T. Wakagi, *FEBS Lett.,* **535** (2003) 200.

8-8 Crystal Structure of a Hydrolase from the Human Malaria Parasite *Plasmodium falciparum*: a Structural Insight into the Rational Design of Selective Inhibitors

Malaria is one of the world's most serious parasitic diseases. There are estimated 300-500 million cases and up to 2.7 million deaths from malaria each year. Human malaria is caused by infection with intracellular parasites of the genus *Plasmodium* that are transmitted by *Anopheles mosquitoes*. *Plasmodium falciparum* is the most lethal among the four species of *Plasmodium* that infect humans. The emergence of strains of malarial parasite resistant to conventional drug therapy has stimulated searches for antimalarials with novel modes of action.

S-adenosyl-L-homocysteine hydrolase (SAHH) [EC 3.3.1.1] catalyzes the reversible hydrolysis of *S*-adenosyl-L-homocysteine to adenosine and L-homocysteine. Recently, SAHH inhibitors are expected to provide new-type chemotherapeutic agents against malaria, because neplanocin A, a strong inhibitor of SAHH, is reported to be a growth inhibitor of *P. falciparum*. The cDNA cloning of *P. falciparum* SAHH (PfSAHH) revealed that the PfSAHH contains a 41-amino acid insert in its sequence as compared with mammalian SAHH. The PfSAHH enzyme, in its active form, is a homo-tetramer of identical subunits, each of which comprises 479 amino acid residues, and contains a tightly but not covalently bound NAD cofactor and has a molecular mass of about 54 kDa. The structural difference between the PfSAHH and mammalian SAHH may give valuable clues for development of antimalarials. The X-ray crystal structures of mammalian (human and rat) SAHHs have been previously reported. However, crystal structures of parasite SAHHs have never been reported. Thus the three-dimensional structure of PfSAHH is essential for the structure-based design of novel selective inhibitors of PfSAHH, which may serve as antimalarial drug leads.

Crystals of PfSAHH were obtained in the presence of a reaction product adenosine (Ado) [1]. The crystals belong to an orthorhombic space group $P2_12_12_1$ with cell dimensions of a = 77.09 Å, b = 86.15 Å, and c = 333.8 Å. Data collection was preformed at PF-AR NW12. The crystal structure has been determined at 2.4 Å resolution by the molecular replacement method using the coordinate set of the human SAHH (HsSAHH) tetramer (PDB code: 1LI4) as a search model [2]. The size of the tetrameric PfSAHH molecule is 65 x 85 x 100 Å and the four subunits are related by a 222 point group symmetry (Fig. 14a). The subunit of PfSAHH consists of two large domains separated by a cleft containing a deep pocket, and a small C-terminal domain that is separated from the main body of the subunit (Fig. 14b). The insert specifically found in PfSAHH is separated from the main body of the tetramer, whereas nucleoside inhibitors of SAHH bind to the crevice of the substrate-binding domain. It is therefore difficult to directly utilize structural information for the insert for a rational design of selective PfSAHH inhibitors. Fortunately, however, knowledge of the present structure of the PfSAHH/Ado complex in combination with a structural comparison with HsSAHH revealed that a single substitution between the PfSAHH (Cys59) and HsSAHH (Thr60) accounts for the differential interactions with nucleoside inhibitors. To examine roles of the Cys59 in the interactions with nucleoside inhibitors, a mutant PfSAHH was prepared [2]. A replacement of Cys59 by Thr results in mutant PfSAHH which shows HsSAHH-like nucleoside inhibitor sensitivity. The present structure should provide opportunities to design potent and selective PfSAHH inhibitors.

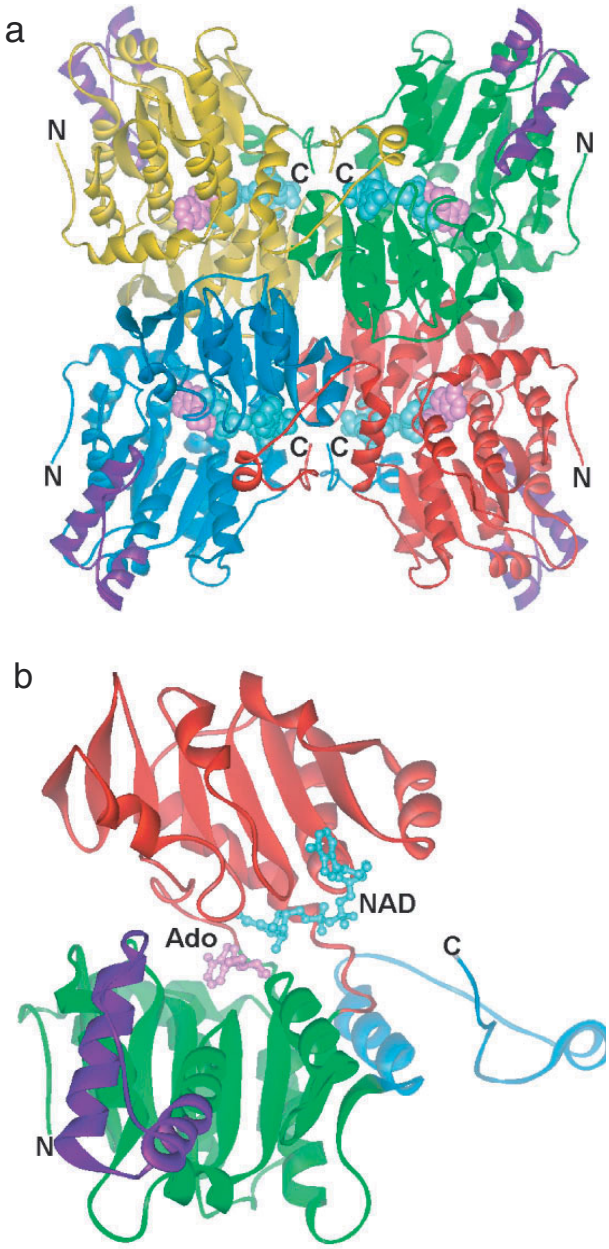

Figure 14
Three-dimensional structure of *Plasmodium falciparum* SAHH (PfSAHH).(a) Front view of the PfSAHH tetramer. The four subunits are shown in different colors. The insertion loop of PfSAHH is shown in violet. The molecules of bound NAD (cyan) and adenosine (Ado, magenta) are shown as space-filling models for each of the four subunits. The N and C termini are marked.(b) Subunit structure of PfSAHH. The subunit is colored green, red, blue, and violet for the substrate-binding domain, the cofactor-binding domain, the C-terminal domain, and the insertion loop, respectively. Bound NAD (cyan) and Ado (pink) molecules are shown as ball-and-stick models. The N and C termini are marked.

N. Tanaka, Y. Kusakabe and K.T. Nakamura (Showa Univ.)

References

[1] N. Tanaka, Y. Kusakabe, K. Shiraiwa, Y. Sakamoto, M. Nakanishi, Y. Kitade and K.T. Nakamura, *Protein Peptide Lett.*,**11** (2004) 201.
[2] N. Tanaka, M. Nakanishi, Y. Kusakabe, K. Shiraiwa, S. Yabe, Y. Ito, Y. Kitade and K.T. Nakamura, *J. Mol. Biol.*, **343** (2004) 1007.

8-9 Solution Structure of the Tandem SH3 Domains of p47^{phox} in an Autoinhibited Form Elucidated by Small Angle X-ray Scattering

The phagocyte NADPH oxidase is a multi-subunit enzyme responsible for the production of reactive oxygen species. The p47^{phox} subunit is a cytosolic component of the oxidase, containing a PX domain, tandem SH3 domains (N-SH3 and C-SH3), a polybasic region/autoinhibitory region (PBR/AIR) and a proline-rich region in this order (Fig. 15A). In resting cells, the tandem SH3 domains of p47^{phox} are masked through an intra-molecular interaction with PBR/AIR, resulting in an autoinhibited form. Upon cell stimulation, a number of serine residues in PBR/AIR are phosphorylated. Phosphorylation of p47^{phox} induces conformational changes that subsequently lead to rearrangements in intra-molecular interactions and the exposure of the tandem SH3 domains that enable interaction with the p22^{phox} subunit in flavocytochrome b_{558}. The interaction plays an important role in the assembly of the activated oxidase complex [1,2].

Recently, the structure of the autoinhibited form of the tandem SH3 domains was determined by X-ray crystallography, which revealed that elongated monomers were related by a crystallographic 2-fold axis at the hinge, forming an intertwisted dimer with a dumbbell-like shape (Fig. 15B) [3,4]. The split half of the intertwisted dimer in the crystal structure was assumed to be physiologically

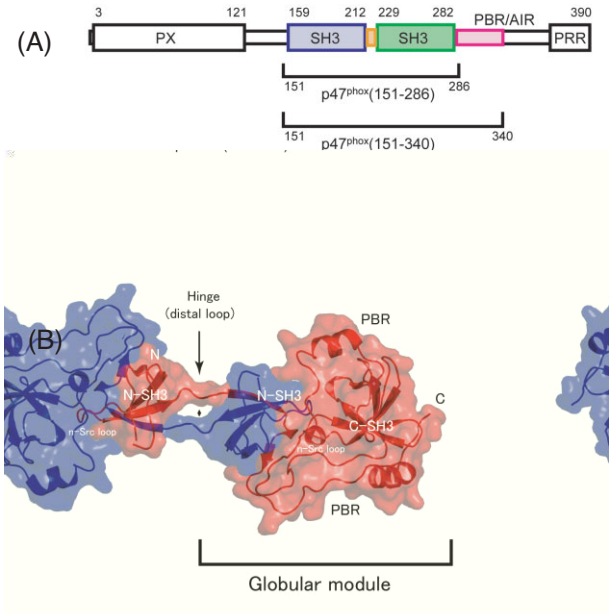

Figure 15
Overall structure of the intertwisted dimer of p47^{phox} in an autoinhibitory form. (A) Domain organization of p47^{phox} showing the PX domain, the tandem SH3 domains (N-SH3 and C-SH3 domain), PBR/AIR and the proline rich region (PRR). (B). Ribbon diagram and surface representation of the intertwisted dimer of p47^{phox}(151-340) (PDB code: 1UEC). One monomer is colored in red and the other in blue.

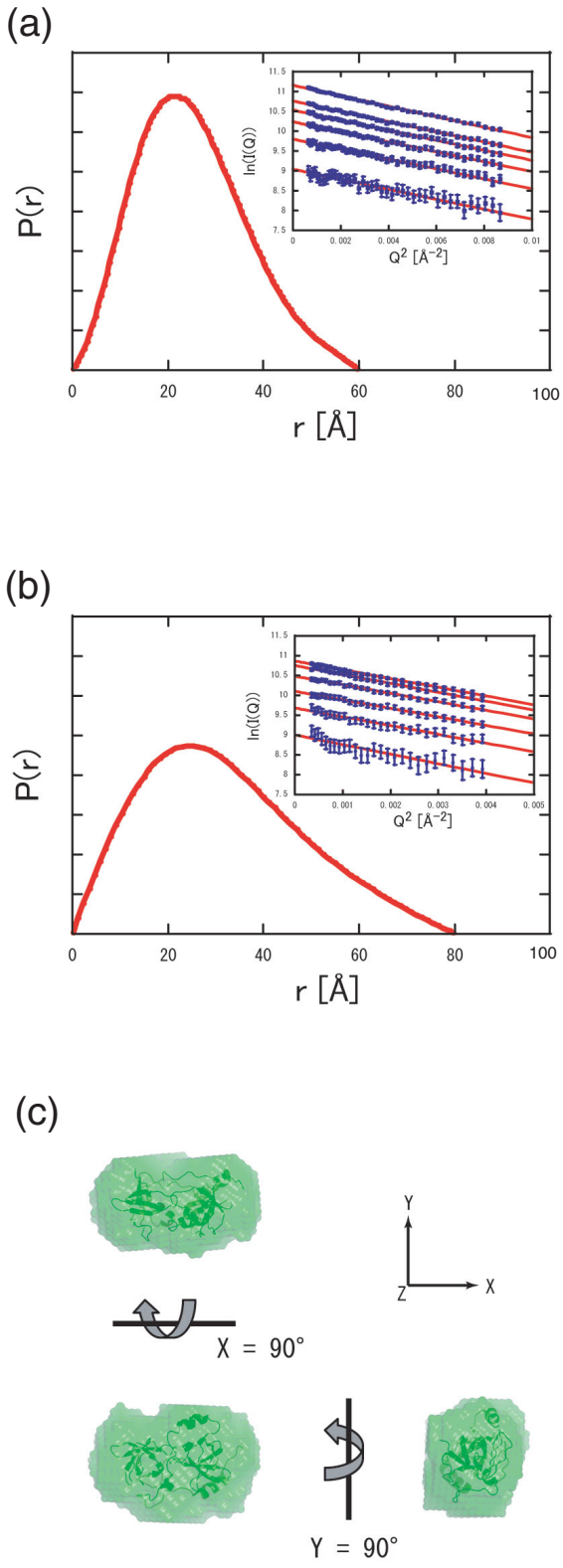

Figure 16
SAXS characterization of the tandem SH3 domains with or without PBR/AIR in p47^{phox}. Distance distribution function, P(r), calculated from the experimental scattering data for p47^{phox}(151-340) (a) and for p47^{phox}(151-286) (b). Guinier region of the scattering curves for p47^{phox}(151-340) (a insert) and for p47^{phox}(151-286) (b insert). (c), Low-resolution model restored by the program DAMMIN which fits to the globular module of p47^{phox}(151-340) (ribbon diagram). The right model is rotated by 90° around the y-axis and the upper model is rotated by 90° around the x-axis according to the arrows.

relevant and to represent the structure of the tandem SH3 domains in the autoinhibited form [3,4], which we called the globular module (Fig. 15B). However, a crucial issue remains to be clarified; whether the globular module exists in solution and if it represents the structure of the autoinhibited form of the tandem SH3 domains. This prompted us to investigate the structural characterization of the tandem SH3 domains in the autoinhibited form in solution [5].

The molecular shapes of the $p47^{phox}$ tandem SH3 domains either with or without PBR/AIR at the C-terminus, were studied using small angle X-ray scattering (SAXS) at PF BL-10C. Considering the SAXS data as well as the molecular mass estimated from the gel filtration analysis and the sedimentation equilibrium analysis, we concluded that both proteins exist as a monomer in solution. R_g of $p47^{phox}$(151-340) was found to be 19.3 Å in contrast to 25.4 Å of $p47^{phox}$(151-286) (Fig. 16 a,b insert), showing that the average molecular dimension of $p47^{phox}$(151-340) is much smaller than that of $p47^{phox}$(151-286). The tandem SH3 domains with PBR/AIR formed a compact globular structure (Fig. 16a), while the tandem SH3 domains lacking the PBR/AIR formed an elongated structure (Fig. 16b). The low-resolution model of $p47^{phox}$(151-340) was determined by *ab initio* molecular shape analysis using the simulated annealing program DAMMIN based on the scattering data of $p47^{phox}$(151-340). The averaged model shown in Fig. 16c roughly fits the globular module in the intertwisted dimer of the crystal structure, with respect to the molecular dimension and molecular shape.

The structure of the globular module represents a solution structure of the tandem SH3 domains in the autoinhibited form. Considering that $p47^{phox}$(151-286) shows a rather extended structure in solution, possibly due to the flexible nature of the linker, PBR/AIR bundles the two SH3 domains and the linker into the globular module which significantly contributes to the stability of $p47^{phox}$(151-340), as shown in the crystalline state. Once PBR/AIR is released by phosphorylation, rearrangements of the SH3 domains may occur, forming an open structure that binds to the cytoplasmic proline rich region of membrane bound $p22^{phox}$.

S. Yuzawa and F. Inagaki (Hokkaido Univ.)

References

[1] B.H. Segal, T.L. Leto, J.I. Gallin, H.L. Malech and S.M. Holland, *Medicine,* **79** (2000) 170.
[2] D.J. Lambeth, *J. Biochem. Mol. Biol.,* **33** (2000) 427.
[3] Y. Groemping, K. Lapouge, S.J. Smerdon and K. Rittinger, *Cell,* **113** (2003) 343.
[4] S. Yuzawa, N.N. Suzuki, Y. Fujioka, K. Ogura, H. Sumimoto and F. Inagaki, *Genes Cells,* **9** (2004) 443.
[5] S. Yuzawa, K. Ogura, M. Horiuchi, N.N. Suzuki, Y. Fujioka, M. Kataoka, H. Sumimoto and F. Inagaki, *J. Biol. Chem.*, **279** (2004) 29752.